

Silica Spheres Coated with $\text{YVO}_4:\text{Eu}^{3+}$ Layers via Sol–Gel Process: A Simple Method To Obtain Spherical Core–Shell Phosphors

M. Yu,[†] J. Lin,^{*,†} and J. Fang[‡]

Key Laboratory of Rare Earth Chemistry and Physics, Changchun Institute of Applied Chemistry, Chinese Academy of Sciences, Changchun 130022, People's Republic of China, and Department of Chemistry and Advanced Materials Research Institute, University of New Orleans, New Orleans, Louisiana 70148

Received November 23, 2004. Revised Manuscript Received January 22, 2005

Spherical SiO_2 particles have been successfully coated with $\text{YVO}_4:\text{Eu}^{3+}$ phosphor layers through a Pechini sol–gel process. The resulted $\text{YVO}_4:\text{Eu}^{3+}@\text{SiO}_2$ core–shell phosphors were characterized by X-ray diffraction (XRD), Fourier-transform IR spectroscopy, scanning electron microscopy, X-ray photoelectron spectra, transmission electron microscopy, UV/vis absorption spectra, general and time-resolved photoluminescence spectra, as well as kinetic decays. The XRD results demonstrate that the $\text{YVO}_4:\text{Eu}^{3+}$ layers begin to crystallize on the SiO_2 particles after annealing at 400 °C, and the crystallinity increases with raising the annealing temperature. The obtained core–shell phosphors have perfect spherical shape with narrow size distribution (average size ca. 500 nm), nonagglomeration, and smooth surface. The thickness of the $\text{YVO}_4:\text{Eu}^{3+}$ shells on SiO_2 cores could be easily tailored by varying the number of deposition cycles (60 nm for two deposition cycles). The Eu^{3+} shows a strong photoluminescence (PL) (dominated by ${}^5\text{D}_0\text{--}{}^7\text{F}_2$ red emission at 617 nm) due to an efficient energy transfer from vanadate groups to Eu^{3+} . The energy transfer process was further studied by the time-resolved emission spectra as well as kinetic decay curves of Eu^{3+} upon excitation into the VO_4^{3-} ion. The PL intensity of Eu^{3+} increases with raising the annealing temperature and the number of coating cycles, and optimum polyethylene glycol concentration in the precursor solution was determined to be 0.08 g/mL for obtaining the strongest emission of Eu^{3+} .

I. Introduction

In recent years, advanced materials derived from core–shell composite particles are of extensive scientific and technological interests due to the ability to fine tune their properties.^{1–5} Core–shell materials consist of a core structural domain covered by a shell domain. The core and shell domains may be composed of a variety of materials including polymers, inorganic solids, and metals. The structure, size, and composition of these particles can be easily altered in a controllable way to tailor their magnetic, optical, mechanical, thermal, electrical, electrooptical, and catalytic properties.^{1–8} The core–shell morphology can be used as a precursor form to produce hollow spheres⁹ or to lower the cost of precious

materials by coating them on inexpensive cores.^{10,11} Core–shell materials can also be used to protect medicines or other materials from dissolution or hydrolysis¹² and to strengthen polymeric materials.¹³ Up to now, many routes have been developed to fabricate such core–shell materials such as sol–gel process,¹ layer-by-layer technique,¹⁴ template-directed self-assembly,¹⁵ and encapsulation of silica nanoparticles by in situ polymerization.¹⁶

On the other hand, the current demand for high-resolution and increased efficiency in phosphors for cathode ray tubes (CRT) and field emissive displays (FEDs) has promoted the development of phosphors that perform at low voltages.¹⁷ In particular, phosphors made up of small, ideally spherical particles are of interest because they offer the possibility of brighter cathodoluminescent performance, high definition, and much improved screen packing.¹⁸ The ideal morphology of phosphor particles includes a perfect spherical (<3 μm) shape, narrow size distribution, and nonagglomeration. Spherical morphology of the phosphors is good for high

* To whom correspondence should be addressed. E-mail: jlin@ns.ciac.jl.cn.

[†] Chinese Academy of Sciences.

[‡] University of New Orleans.

- (1) Caruso, R. A.; Antonietti, M. *Chem. Mater.* **2001**, *13*, 3272.
- (2) Caruso, F.; Spasova, M.; Salgueirino-Macera, V. *Adv. Mater.* **2001**, *13*, 1090. Caruso, F.; Lichtenfeld, H.; Mohwald, H. *J. Am. Chem. Soc.* **1998**, *120*, 8523. Caruso, F.; Caruso, R.; Mohwald, H. *Science* **1998**, *282*, 1111.
- (3) Jiang, Z. H.; Liu, C. Y. *J. Phys. Chem. B* **2003**, *107*, 12411.
- (4) Sertchook, H.; Avnir, D. *Chem. Mater.* **2003**, *15*, 1690.
- (5) Giersig, M.; Ung, T.; Liz-Marzan, L. M.; Mulvaney, P. *Adv. Mater.* **1997**, *9*, 570.
- (6) Ung, T.; Liz-Marzan, L. M.; Mulvaney, P. *Langmuir* **1998**, *14*, 3740.
- (7) Oldenburg, S. J.; Averitt, R. D.; Westcott, S. L.; Halas, N. J. *Chem. Phys. Lett.* **1998**, *288*, 243.
- (8) Fleming, M. S.; Mandal, T. K.; Walt, D. R. *Chem. Mater.* **2001**, *13*, 2210.
- (9) Zhong, Z. Y.; Yin, Y. D.; Gates, B.; Xia, Y. N. *Adv. Mater.* **2000**, *12*, 206.

- (10) Ocana, M.; Hsu, W. P.; Matijevic, E. *Langmuir* **1991**, *7*, 2911.
- (11) Hsu, W. P.; Yu, R. C.; Matijevic, E. *J. Colloid Interface Sci.* **1993**, *156*, 56.
- (12) Lee, J. H.; Park, T. G.; Chol, H.-K. *J. Microencapsulation* **1999**, *16*, 715.
- (13) Schirrer, R.; Lenke, R.; Boudouaz, J. *Polym. Eng. Sci.* **1997**, *37*, 1748.
- (14) Schuetzand, P.; Caruso, F. *Chem. Mater.* **2002**, *14*, 4509.
- (15) Hall, S. R.; Davis, S. A.; Mann, S. *Langmuir* **2000**, *16*, 1454.
- (16) Sondi, I.; Fedynshyn, T. H.; Sinta, R.; Matijevic, E. *Langmuir* **2000**, *16*, 9031.
- (17) Martinez-Rubio, M. I.; Ireland, T. G.; Fern, G. R.; Silver, J.; Snowden, M. J. *Langmuir* **2001**, *17*, 7145.

brightness and high resolution. Additionally, high packing densities and low scattering of light can also be obtained by using spherical phosphors. Nowadays, many synthetic routes have been developed to control the size and distribution of phosphor particles, such as spray pyrolysis¹⁹ and fluxes precipitation.²⁰

Silica can be easily made controllably in spherical morphology from nano- to micrometer size.²¹ If the silica spheres are coated with layers of phosphors, a kind of core-shell phosphor materials with spherical morphology will be obtained, and the size for the phosphor particles can be controlled by the silica cores. Furthermore, because silica is cheaper than most of the phosphor materials (which often employ the expensive rare-earth elements as the activators and/or host components), the core-shell phosphor materials will be cheaper than the pure phosphor materials in unit mass. However, so far this kind of core-shell phosphor materials has not been reported in the literature. Our group has been preparing various kinds of phosphor coatings on bulk silica glass and silicon wafer substrates via the sol-gel process.²² It would be of great interest and importance to check if the core-shell phosphor materials can be prepared in a similar process. Eu^{3+} -activated YVO_4 is an important commercial red phosphor used in color television and the high-pressure mercury lamp, which was first reported by Levine and Palilla.²³ Recently, the preparation and optical properties of nanocrystalline $\text{YVO}_4:\text{Eu}^{3+}$ ^{24, 25} and related $\text{LaPO}_4:\text{Eu}^{3+}$ (Ce^{3+} , Tb^{3+})/ LaPO_4 core-shell nanocrystals²⁶ as well as $\text{LaPO}_4:\text{Ce}^{3+}$, Tb^{3+} nanocrystals conjugated to protein²⁷ or assembled on polystyrene spheres¹⁴ have attracted great interests for potentially biological labeling applications.

Herein, we select $\text{YVO}_4:\text{Eu}^{3+}$ as the phosphor shells and silica spheres as the cores, respectively, to obtain the core-shell structured $\text{YVO}_4:\text{Eu}^{3+}@\text{SiO}_2$ materials via the sol-gel process and characterize the structure, morphology, and photoluminescent properties of the resulting samples.

II. Experimental Section

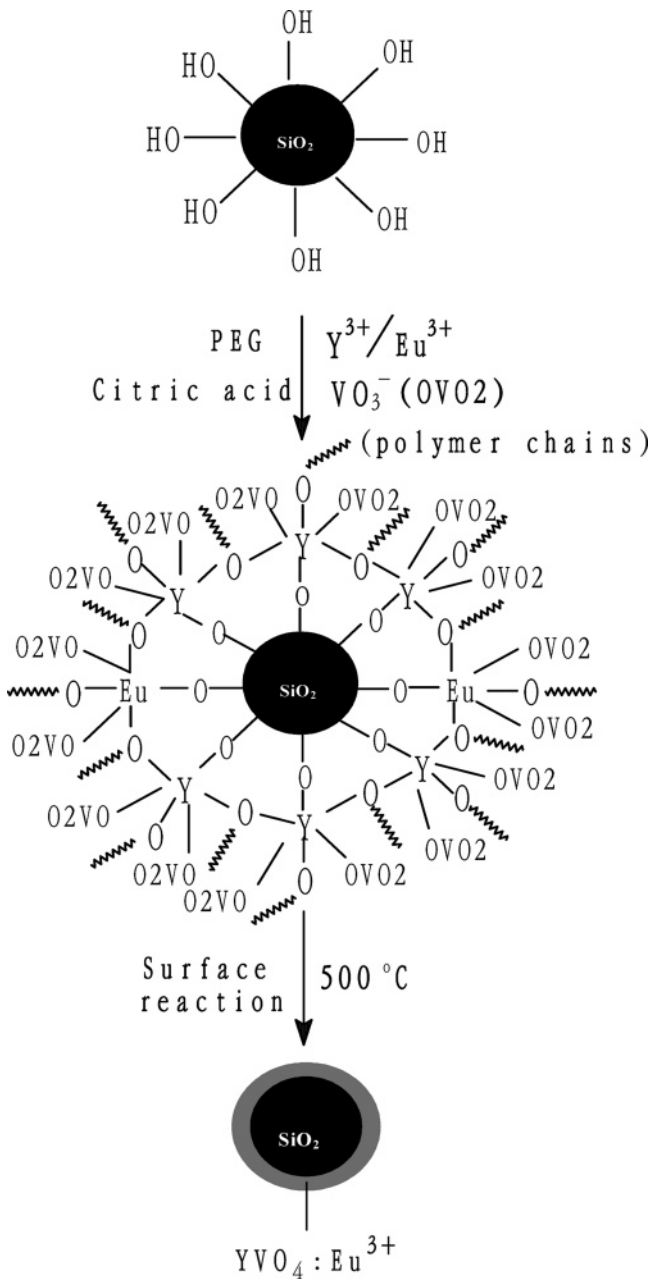
Synthesis of Silica Cores. Amorphous sub-micrometer spheres of silica in the size range of 500–600 nm were synthesized by base-catalyzed hydrolysis of tetraethoxysilane (TEOS) via the well-known Stöber process, i.e., the hydrolysis of TEOS in an ethanol solution containing water and ammonia.²¹ This method yielded the colloidal solution of silica particles with a narrow size distribution in the sub-micrometer range, and the particle size of silica depended on relative concentration of the reactants. In a typical experiment, 21 mL of TEOS (99 wt. %, analytical reagent, (AR)), 9 mL of deionized H_2O , and 245 mL of NH_4OH (25 wt. %, AR) were added into 225 mL of absolute ethanol and stirred at room temperature for 4 h, resulting in the formation of white silica colloidal suspension. The silica particles were centrifugally separated from the suspension and washed with ethanol for four times.

Coating of SiO_2 Cores with $\text{YVO}_4:\text{Eu}^{3+}$ Shells. SiO_2 core- $\text{YVO}_4:\text{Eu}^{3+}$ shell particles ($\text{YVO}_4:\text{Eu}^{3+}@\text{SiO}_2$) were prepared by a Pechini sol-gel process.²² The doping concentration of Eu^{3+} was 5 mol % that of Y^{3+} in YVO_4 host ($\text{Y}_{0.95}\text{Eu}_{0.05}\text{VO}_4$), which had been optimized previously.^{24,25} Stoichiometric weights of Y_2O_3 (99.99%), Eu_2O_3 (99.99%), and NH_4VO_3 (99%, AR) were dissolved in dilute HNO_3 (AR) and then were mixed with a water-ethanol ($v/v = 1:7$) solution containing citric acid (AR) as a chelating agent for the metal ions. The molar ratio of metal ions to citric acid was 1:2. As a cross-linking agent, polyethylene glycol (PEG, molecular weight = 10 000, AR) was added with a final concentration ranging from 0.04 to 0.20 g/mL. The solution was stirred for 1 h to form a sol, and then the silica particles were added under stirring. The suspension was further stirred for another 3 h, then the silica particles were separated by centrifugation. The samples were dried at 100 °C for 1 h immediately. Then the dried samples were annealed to the desired temperature (300–700 °C) with a heating rate of 1 °C/min and held there for 2 h in air. The above process was repeated for several times to increase the thickness of the $\text{YVO}_4:\text{Eu}^{3+}$ shells. In this way, the core-shell structured $\text{YVO}_4:\text{Eu}^{3+}@\text{SiO}_2$ materials have been obtained, and the whole process is shown in Scheme 1. For the purpose of comparison, the coating sol was evaporated to form powders, which were annealed in a similar process to produce the pure $\text{YVO}_4:\text{Eu}^{3+}$ powder phosphors.

Characterization. The X-ray diffraction (XRD) of the powder samples was examined on a Rigaku-Dmax 2500 diffractometer using $\text{Cu K}\alpha$ radiation ($\lambda = 0.154\ 05\ \text{nm}$). Fourier-transform IR spectra were measured with a Perkin-Elmer 580B IR spectrophotometer with the KBr pellet technique. The morphology of the samples was inspected using a scanning electron microscope (JEOL JXA-840) and a transmission electron microscope (JEOL-2010, 200 kV). The X-ray photoelectron spectra (XPS) were taken on a VG ESCALAB MK II electron energy spectrometer using $\text{Mg K}\alpha$ (1253.6 eV) as the X-ray excitation source. The UV/vis absorption spectra were measured on a TU-1901 spectrophotometer. The excitation and emission spectra were taken on a Hitachi F-4500 spectrofluorimeter equipped with a 150-W xenon lamp as the excitation source. Time-resolved photoluminescence spectra and luminescence decay curves were obtained from a Lecroy Wave Runner 6100 Digital Oscilloscope (1GHz) using a 278-nm laser (pulse width = 4 ns, gate = 50 ns) as the excitation source

- (18) Jing, X.; Ireland, T. G.; Gibbons, C.; Barber, D. J.; Silver, J.; Vecht, A.; Fern, G.; Trogwa, P.; Morton, D. *J. Electrochem. Soc.* **1999**, *146*, 4546. Vecht, A.; Gibbons, C.; Davies, D.; Jing, X.; Marsh, P.; Ireland, T. G.; Silver, J.; Newport, A.; *J. Vac. Sci. Technol. B* **1999**, *17*, 750. Jiang, Y. D.; Wang, Z. L.; Zhang, F.; Paris, H. G.; Summers, C. J. *J. Mater. Res.* **1998**, *13*, 2950.
- (19) Jung, K. Y.; Lee, D. Y.; Kang, Y. C.; Park, H. D. *J. Lumin.* **2003**, *105*, 127. Kang, Y. C.; Lenggono, I. W.; Park, S. B.; Okuyama K. *Mater. Res. Bull.* **2000**, *35*, 789. Zhou, Y. H.; Lin, J.; Han, X. M.; Wang, S. B.; Zhang, H. J. *Mater. Res. Bull.* **2003**, *38*, 1289. Cho, S. H.; Yoo, J. S.; Lee, J. D. *J. Electrochem. Soc.* **1998**, *145*, 1017. Xu, C.; Watkins, B. A.; Sievers, R. E.; Jing, X.; Trwoga, P.; Gibbons, C. S.; Vecht, A. *Appl. Phys. Lett.* **1997**, *71*, 1643.
- (20) Celikkaya, A.; Akinc, M. *J. Am. Ceram. Soc.* **1990**, *73*, 2360.
- (21) Stöber, W.; Fink, A.; Bohn, E. *J. Colloid Interface Sci.* **1968**, *26*, 62. Jiang, P.; Bertone, J. F.; Hwang, K. S.; Colvin, V. L. *Chem. Mater.* **1999**, *11*, 2132.
- (22) Pang, M. L.; Lin, J.; Yu, M.; Wang, S. B. *J. Solid State Chem.* **2004**, *177*, 2236. Yu, M.; Lin, J.; Fu, J.; Zhang, H. J.; Han, Y. C. *J. Mater. Chem.* **2003**, *13*, 1413. Yu, M.; Wang, Z.; Fu, J.; Wang, S.; Zhang, H. J.; Han, Y. C. *Chem. Mater.* **2002**, *14*, 2224. Yu, M.; Lin, J.; Zhou, Y. H.; Wang, S. B.; Zhang, H. J. *J. Mater. Chem.* **2002**, *12*, 86. Lin, J.; Sanger, D. U.; Mennig, M.; Baerner, K. *Thin Solid Films* **2000**, *360*, 39.
- (23) Levine, A. K.; Palilla, F. C. *Appl. Phys. Lett.* **1964**, *5*, 118
- (24) Huignard, A.; Gacoin, T.; Boilot, J.-P. *Chem. Mater.* **2000**, *12*, 1090. Huignard, A.; Buisette, V.; Laurent, G.; Gacoin, T.; Boilot, J.-P. *Chem. Mater.* **2002**, *14*, 2264. Huignard, A.; Buisette, V.; Franville, A.-C.; Gacoin, T.; Boilot, J.-P. *J. Phys. Chem. B* **2003**, *107*, 6754. Yan, C. H.; Sun, L. D.; Liao, C. S. *Appl. Phys. Lett.* **2003**, *82*, 3511.
- (25) Riwozki, K.; Haase, M. *J. Phys. Chem. B* **2001**, *105*, 12709. Haase, M.; Riwozki, K.; Meyssamy, H.; Kornowski, A. *J. Alloys Compd.* **2000**, *303*, 191.
- (26) Lehmann, O.; Kömpe, K.; Haase, M. *J. Am. Chem. Soc.* **2004**, *126*, 14935. Kömpe, K.; Borchert, H.; Storz, J.; Lobo, A.; Adam, S.; Möller, T.; Haase, M. *Angew. Chem., Int. Ed.* **2003**, *42*, 5513.
- (27) Meiser, F.; Cortez, C.; Caruso, F. *Angew. Chem., Int. Ed.* **2004**, *43*, 5954.

Scheme 1. Formation Process of $\text{YVO}_4:\text{Eu}^{3+} @\text{SiO}_2$ Core-Shell Particles



(Continuum Sunlite OPO). All the measurements were performed at room temperature.

III. Results and Discussion

Formation and Morphology of $\text{YVO}_4:\text{Eu}^{3+} @\text{SiO}_2$ Core-Shell Particles. XRD. XRD study revealed that the both the as-formed silica particles and the 300°C annealed core-shell particles are amorphous, and the core-shell particles begin to crystallize after annealing at 400°C . Figure 1 shows the XRD patterns for the 500°C annealed SiO_2 (a), $\text{YVO}_4:\text{Eu}^{3+} @\text{SiO}_2$ (b), pure $\text{YVO}_4:\text{Eu}^{3+}$ (c) powder samples as well as the JCPDS card (No. 17-341) for YVO_4 (d) as a reference. For SiO_2 particles annealed at 500°C (Figure 1a), no diffraction peak is observed except for a broad band centered at $2\theta = 22.00^\circ$, which is the characteristic peak for amorphous SiO_2 (JCPDS 29-0085). For the $\text{YVO}_4:\text{Eu}^{3+} @\text{SiO}_2$

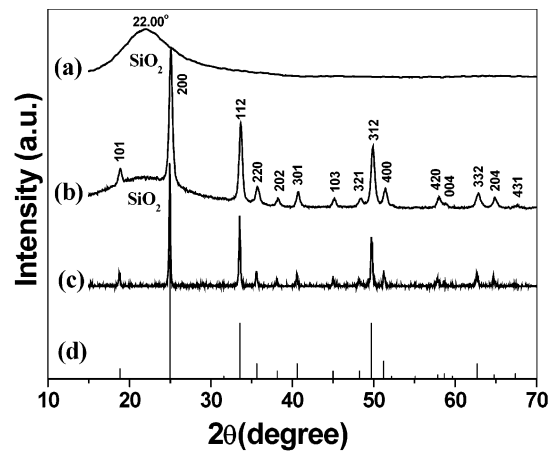


Figure 1. XRD patterns for SiO_2 (a), $\text{YVO}_4:\text{Eu}^{3+} @\text{SiO}_2$ core-shell particles (b), pure $\text{YVO}_4:\text{Eu}^{3+}$ powders (c), and the JCPDS card 17-341 for YVO_4 (d). All the samples were obtained after annealing at 500°C for 2 h.

core-shell sample fired at 500°C (Figure 1b), besides the broad band at $2\theta = 22.00^\circ$ from amorphous SiO_2 , all the diffraction peaks belonging to crystalline YVO_4 are present, suggesting that the coatings of $\text{YVO}_4:\text{Eu}^{3+}$ have crystallized well on the surfaces of amorphous silica particles. This is in good agreement with the situation for the pure $\text{YVO}_4:\text{Eu}^{3+}$ powder sample annealed at 500°C (Figure 1c, in which well crystalline YVO_4 is observed). No other phase is detected for $\text{YVO}_4:\text{Eu}^{3+} @\text{SiO}_2$ core-shell samples even after annealing at 700°C (which only increases the intensity of the diffraction peaks of YVO_4 to some extent due to the improvement of crystallinity).

It is interesting to note that the diffraction peaks of YVO_4 in $\text{YVO}_4:\text{Eu}^{3+} @\text{SiO}_2$ core-shell samples (Figure 1b) are broader than those of the pure $\text{YVO}_4:\text{Eu}^{3+}$ powder (Figure 1c), indicating that the crystallite size of $\text{YVO}_4:\text{Eu}^{3+}$ grains on the surfaces of the silica particles is smaller than that in the pure powders of $\text{YVO}_4:\text{Eu}^{3+}$. In general, the nanocrystallite size can be estimated from the Scherrer equation, $D = 0.941\lambda/\beta \cos \theta$, where D is the average grain size, λ is the X-ray wavelength (0.15405 nm), and θ and β are the diffraction angle and full-width at half-maximum (in radian) of an observed peak, respectively.²⁸ The strongest peak (200) at $2\theta = 25.0^\circ$ was used to calculate the average crystallite size (D) of $\text{YVO}_4:\text{Eu}^{3+}$ on the surfaces of silica particles and in the pure $\text{YVO}_4:\text{Eu}^{3+}$ powders. The estimated average crystallite sizes are 20 nm for the former and 50 nm for the latter, respectively. Furthermore, the calculated crystal cell parameters ($a = 0.710 \text{ nm}$, $c = 0.628 \text{ nm}$, $V = 0.316 \text{ nm}^3$) for the crystalline $\text{YVO}_4:\text{Eu}^{3+}$ in the $\text{YVO}_4:\text{Eu}^{3+} @\text{SiO}_2$ core-shell sample are a little smaller than those ($a = 0.725 \text{ nm}$, $c = 0.629 \text{ nm}$, $V = 0.330 \text{ nm}^3$) in the pure $\text{YVO}_4:\text{Eu}^{3+}$ powder. This may be caused by slightly different crystallization behaviors of $\text{YVO}_4:\text{Eu}^{3+}$ on the silica surfaces and in pure $\text{YVO}_4:\text{Eu}^{3+}$ powders. The above results and the

(28) Zhang, Y. W.; Jin, S.; Tian, S. J.; Li, G. B.; Jia, T.; Liao, C. S.; Yan, C. H. *Chem. Mater.* **2001**, *13*, 372. Nedelec, J. M.; Avignand, D.; Mahiou, R. *Chem. Mater.* **2002**, *14*, 651.

(29) Kioul, A.; Mascia, L. *J. Non-Cryst. Solids* **1994**, *175*, 169. Kook Mah, S.; Chung, I. J. *J. Non-Cryst. Solids* **1995**, *183*, 252. Chen, Y.; Iroh, J. O. *Chem. Mater.* **1999**, *11*, 1218. Méndez-Vivar, J.; Mendoza-Bandala, A. *J. Non-Cryst. Solids* **2000**, *261*, 127.

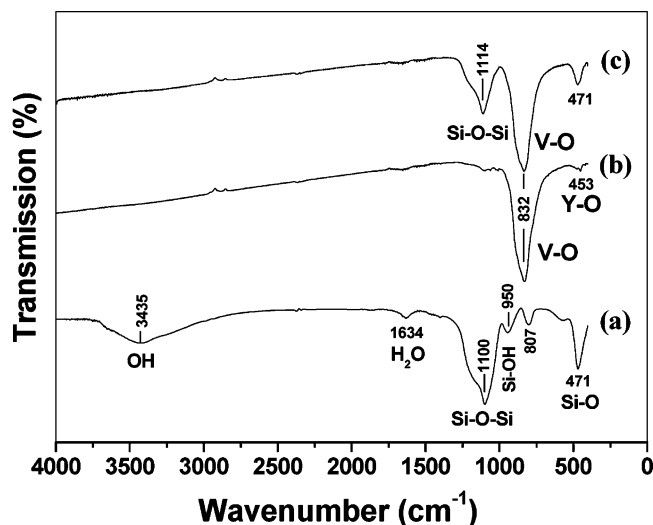


Figure 2. FT IR spectra of the as-formed SiO₂ (a), 500 °C annealed YVO₄:Eu³⁺ powder (b), and YVO₄:Eu³⁺@SiO₂ core-shell samples (c).

structural characteristics for YVO₄:Eu³⁺ are collected in Table 1.

FT IR. The FT IR spectra of the as-formed SiO₂, 500 °C annealed pure YVO₄:Eu³⁺ powder and YVO₄:Eu³⁺@SiO₂ core-shell samples are shown in parts a–c of Figure 2, respectively. In Figure 2a for the as-formed SiO₂ particles, the absorption bands due to OH (3435 cm⁻¹), H₂O (1634 cm⁻¹), Si–O–Si (ν_{as} , 1100 cm⁻¹; ν_s , 807 cm⁻¹), Si–OH (ν_s , 950 cm⁻¹), and Si–O (δ , 471 cm⁻¹) bonds (where ν_{as} = asymmetric stretching, ν_s = symmetric stretching, δ = bending) are observed.²⁹ This indicates that the as-formed SiO₂ particles contain a large amount of OH groups and H₂O on their surfaces.⁴ The surface Si–OH groups play an important role for bonding the metal ions (Y³⁺, Eu³⁺) from the coating sol and forming the YVO₄:Eu³⁺ layers on the SiO₂ surfaces in the following annealing process, as shown in Scheme 1. In Figure 2b for pure YVO₄:Eu³⁺ powders, a strong absorption peak at 832 cm⁻¹ and a weak one at 453 cm⁻¹ have appeared, which are attributed to the absorption of V–O (from VO₄³⁻ group) and Y(Eu)–O bonds, respectively.²² This suggests that crystalline phase (YVO₄) has formed after annealing at 500 °C, agreeing well with the results of XRD. For the YVO₄:Eu³⁺@SiO₂ core-shell sample (Figure 2c), the characteristic absorption peaks of the V–O bond (832 cm⁻¹) for YVO₄:Eu³⁺ (Figure 2b) and the Si–O–Si bond (1114 cm⁻¹) for amorphous SiO₂ (Figure 2a) have been observed clearly, and the weak signal from the Y–O bond may be covered by the bending vibration of

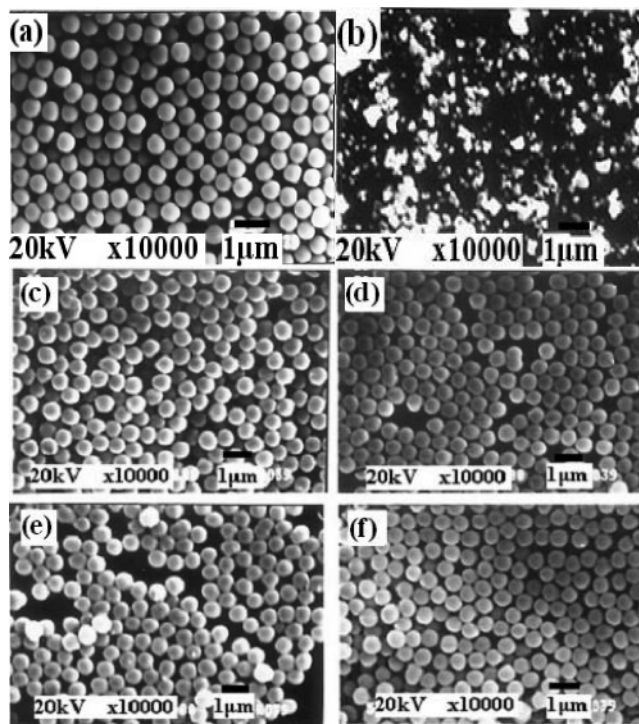


Figure 3. SEM micrographs of the as-formed SiO₂ (a), 500 °C annealed YVO₄:Eu³⁺ powder (b), and the SiO₂ particles coated with one (c), two (d), three (e), and four (f) layers of YVO₄:Eu³⁺, respectively.

Si–O bond at 471 cm⁻¹. The signal of OH groups from the as-formed silica particles have disappeared completely in the 500 °C annealed YVO₄:Eu³⁺@SiO₂ core-shell particles. These results are consistent with those of XRD and further demonstrate the formation of crystalline YVO₄:Eu³⁺ coatings on the silica surfaces via the sol–gel deposition and annealing process.

SEM, XPS, and TEM. Figure 3 shows the SEM micrographs of the as-formed SiO₂ particles (a), the pure YVO₄:Eu³⁺ powders (b), and SiO₂ particles coated by 1–4 layers of YVO₄:Eu³⁺ (c–f), respectively. From the SEM micrograph of Figure 3a, we can observe that the as-formed SiO₂ consists of spherical particles with an average size of 500 nm, and these particles are nonaggregated with narrow size distribution. On the contrary, the pure YVO₄:Eu³⁺ powders contain irregular particles with wide size distribution (150–500 nm), as shown in Figure 3b. After the silica particles were functionalized by YVO₄:Eu³⁺ coatings, the resulting YVO₄:Eu³⁺@SiO₂ particles still keep the morphological properties of the silica particles, i.e., these particles are still spherical and nonaggregated but slightly larger than the pure silica particles due to the additional layers of YVO₄:Eu³⁺ on them, as shown in parts c–f of Figure 3. Moreover, the irregular fine particles such as the pure YVO₄:Eu³⁺ powders in Figure 3b cannot be observed in parts c–f of Figure 3. This indicates that all of the YVO₄:Eu³⁺ materials have been coated on the surfaces of silica particles by our experimental process. However, it should be mentioned that the SEM micrographs can only provide the basic information on the morphology of YVO₄:Eu³⁺@SiO₂ particles in the large scale (namely, all of the SiO₂ particles remain spherical and nonaggregated after being subjected to the sol–gel coating of YVO₄:Eu³⁺ layers on them), and

Table 1. Crystallite Sizes, Cell Parameters, and Structural Characteristics for YVO₄:Eu³⁺ in YVO₄:Eu³⁺@SiO₂ Spheres and YVO₄:Eu³⁺ Powders

YVO ₄ :Eu ³⁺	core-shell spheres	pure powders
crystallite size	20 nm	50 nm
crystal cell parameters	$a = 0.710$ nm	$a = 0.725$ nm
	$c = 0.628$ nm	$c = 0.629$ nm
	$V = 0.316$ nm ³	$V = 0.330$ nm ³
crystal system	tetragonal	
space group	$I4_1/amd$	
coordination environment of Y ³⁺ (Eu ³⁺)	8(O), all the O atoms belong to VO ₄ tetrahedra	
site symmetry of Y ³⁺ (Eu ³⁺)	D_{2d}	

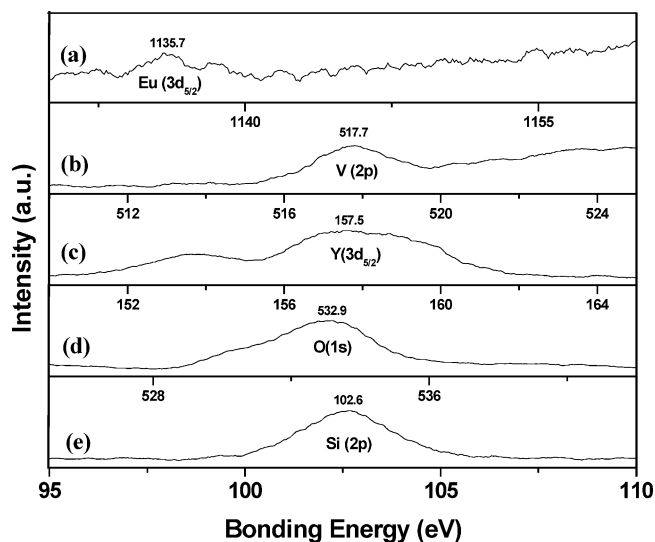


Figure 4. XPS of $\text{YVO}_4:\text{Eu}^{3+}@\text{SiO}_2$ core-shell particles.

the core-shell structure of $\text{YVO}_4:\text{Eu}^{3+}@\text{SiO}_2$ particles cannot be resolved from the SEM micrographs due to the low magnification.

To further confirm the existence of $\text{YVO}_4:\text{Eu}^{3+}$ layers on the surfaces of silica particles, the sample in Figure 3c was subjected to XPS analysis, which is a powerful tool for determining the surface composition of a material qualitatively. Figure 4 shows the XPS analysis result of the sample. Signals of bonding energy from the Eu ($3d_{5/2}$, 1134.7 eV), V ($2p$, 517.7 eV), Y ($3d_{5/2}$, 157.5 eV), O ($1s$, 532.9 eV), and Si ($2p$, 102.6 eV) can be seen clearly in parts a–e of Figure 4, respectively.³⁰ By combination of the previous results of XRD and FT IR, we can deduce that these signals arise from the $\text{YVO}_4:\text{Eu}^{3+}$ shells (a–d) and SiO_2 cores (d–e) of the sample, respectively. This provides additional evidence for the formation of coatings of crystalline $\text{YVO}_4:\text{Eu}^{3+}$ on the SiO_2 particles.

To see the core-shell structure of $\text{YVO}_4:\text{Eu}^{3+}@\text{SiO}_2$ particles, TEM was performed. Representative TEM micrographs for the SiO_2 particles coated by two times (layers) of $\text{YVO}_4:\text{Eu}^{3+}$ shells as well as for the pure SiO_2 particles (as reference) are shown in parts a–d of Figure 5, respectively. In Figure 5a, the core-shell structure for the $\text{YVO}_4:\text{Eu}^{3+}@\text{SiO}_2$ particles can be seen clearly due to the different electron penetrability for the cores and shells. The cores are black spheres with an average size of 500 nm (similar to the pure SiO_2 particles in Figure 5d), and the shells have gray color with an average thickness of 60 nm. The high-resolution TEM and electron diffraction measurements were performed in the interface region of the core and shell of a particle as labeled in Figure 5a, and the micrographs are shown in parts b and c of Figure 5, respectively. The lattice fringes of crystalline phase ($\text{YVO}_4:\text{Eu}^{3+}$) can be seen clearly in Figure 5b, and the electron diffraction rings with some disorder in Figure 5c just demonstrate the coexistence of crystalline phase ($\text{YVO}_4:\text{Eu}^{3+}$) and amorphous phase (SiO_2) in the interface region of the core-shell particle.

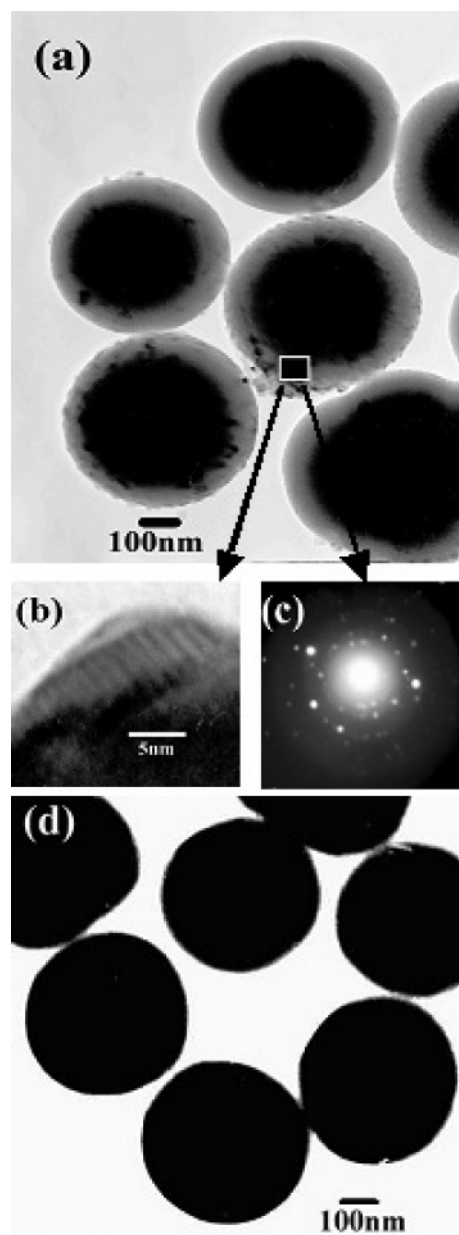


Figure 5. TEM micrographs of SiO_2 coated with two layers of $\text{YVO}_4:\text{Eu}^{3+}$ (a), high-resolution TEM (b), electron diffraction pattern for the selective interface region of the particle in part a (c), and the bare SiO_2 particles (d).

Photoluminescence Properties. Spectral and Kinetic Properties of $\text{YVO}_4:\text{Eu}^{3+}@\text{SiO}_2$ Core-Shell Phosphors. The obtained $\text{YVO}_4:\text{Eu}^{3+}@\text{SiO}_2$ core-shell phosphor particles can be dispersed in ethylene glycol to form a relatively stable colloid, whose UV/vis absorption spectrum was measured, as shown in Figure 6a. A strong absorption band peaking at 278 nm is observed, agreeing well with the reported absorption spectra of colloid solution of nanocrystalline $\text{YVO}_4:\text{Eu}$.^{24,25} Obviously, this band is ascribed to a charge transfer from the oxygen ligands to the central vanadium atom within the VO_4^{3-} group ions. From the viewpoint of molecular orbital theory, it corresponds to transitions from the $^1A_2(^1T_1)$ ground state to $^1A_1(^1E)$ and $^1E(^1T_2)$ excited states of VO_4^{3-} ion.³¹

(30) Reddy, B. M.; Lakshmanan, P.; Khan, A. *J. Phys. Chem. B* **2004**, *108*, 16855. Chatterjee, T.; McCann, P. J.; Fang, X. M.; Johnson, M. B. *J. Vac. Sci. Technol. B* **1998**, *16*, 1463. Wu, L.; Yu, J. C.; Zhang, L. Z.; Wang, X. C.; Li, S. K. *J. Solid State Chem.* **2004**, *177*, 3666.

(31) Hsu, C.; Powell, R. C. *J. Lumin.* **1975**, *10*, 273.

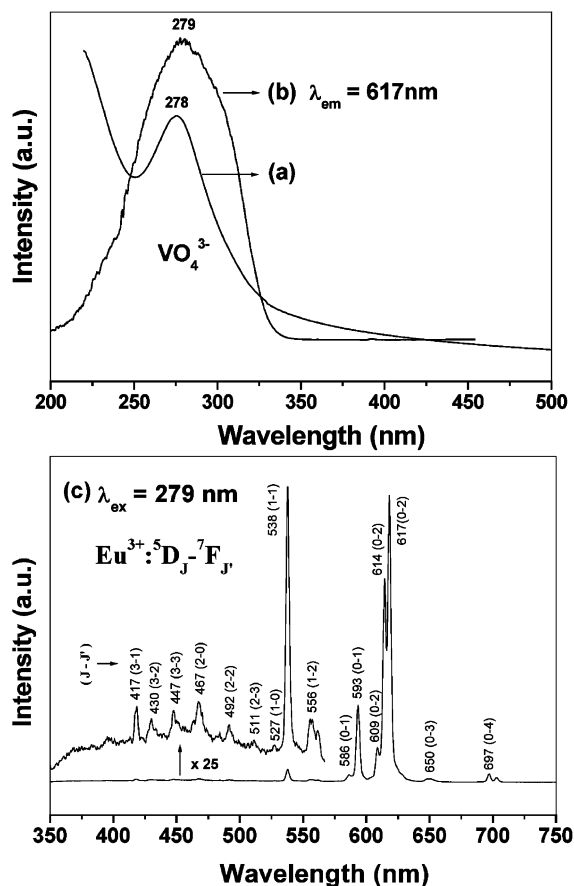


Figure 6. Absorption (a), excitation (b), and emission (c) spectra of $\text{YVO}_4:\text{Eu}^{3+}@\text{SiO}_2$ core-shell particles. The absorption spectrum was taken on the colloid solution of $\text{YVO}_4:\text{Eu}^{3+}@\text{SiO}_2$ particles dispersed in ethylene glycol.

Upon UV excitation, the $\text{YVO}_4:\text{Eu}^{3+}@\text{SiO}_2$ core-shell phosphors exhibit strong red luminescence. Parts b and c of Figure 6 show the excitation and emission spectra of the core-shell phosphors annealed at 500 °C, respectively. In agreement with the absorption spectrum in Figure 6a, the excitation spectrum (Figure 6b) monitored with 617-nm emission of Eu^{3+} (${}^5\text{D}_0\text{--}{}^7\text{F}_2$) consists of a strong absorption band with a maximum at 279 nm due to the VO_4^{3-} ion.²⁴ The general f-f transition lines of Eu^{3+} in the longer wavelength region have not been observed due to their weak intensity relative to that of the VO_4^{3-} . This indicates that the excitation of Eu^{3+} is mainly through the VO_4^{3-} ions, i.e., by energy transfer from VO_4^{3-} to Eu^{3+} . Excitation into the VO_4^{3-} group at 279 nm yields the emission spectrum (Figure 6c), which not only contains the characteristic transition lines from the lowest excited ${}^5\text{D}_0$ level of Eu^{3+} but also those from higher energy levels (${}^5\text{D}_1$, ${}^5\text{D}_2$, ${}^5\text{D}_3$) of Eu^{3+} with a very weak intensity (which can be seen more clearly by enlarging the emission spectrum in the short wavelength region). No emission from the VO_4^{3-} group is observed, suggesting that the energy transfer from VO_4^{3-} to Eu^{3+} is very efficient. The locations for the main emission lines of Eu^{3+} and their assignments are labeled in the figure. Obviously, the emission spectrum is dominated by the red ${}^5\text{D}_0\text{--}{}^7\text{F}_2$ hypersensitive transition of Eu^{3+} due to the low local symmetry (D_{2d} , without inversion center, Table 1) for the sites of Eu^{3+} in the YVO_4 host lattices.²² Note that the ${}^5\text{D}_0\text{--}{}^7\text{F}_0$ transition of

Eu^{3+} (which is only allowed for C_s , C_n , C_{nv} site symmetry³²) is absent in the emission spectrum. In addition, the crystal field splitting of $\text{Eu}^{3+} {}^5\text{D}_0\text{--}{}^7\text{F}_{1, 2, 4}$ transitions can be seen clearly, indicating that the sample is well crystallized. In general silicate host lattices with high phonon energy (1100 cm^{-1} , the vibration frequency of Si-O-Si bond), the emission from the higher energy levels (${}^5\text{D}_1$, ${}^5\text{D}_2$, ${}^5\text{D}_3$) of Eu^{3+} is quenched completely by the multiphonon relaxation process.³³ However, in $\text{YVO}_4:\text{Eu}^{3+}@\text{SiO}_2$ core-shell phosphors the emission from higher excited states of Eu^{3+} is present despite the high-energy phonons of Si-O-Si from the SiO_2 cores (1114 cm^{-1} , Figure 2c). This indicates that the SiO_2 cores have little influence on the luminescence properties of the phosphors due to the long distance of between Si-O-Si networks and the Eu^{3+} ions. The emission properties of Eu^{3+} are mainly determined by the nearest coordinated VO_4^{3-} ions, whose lower vibration energy (832 cm^{-1}) is not able to bridge the gaps between the higher energy levels and ${}^5\text{D}_0$ level of Eu^{3+} completely, resulting in the weak emission from these levels. All the above spectral properties for the $\text{YVO}_4:\text{Eu}^{3+}@\text{SiO}_2$ core-shell phosphors are basically consistent with the reported bulk,^{23,34} nanocrystalline powder,^{24,25} and thin film³⁵ of $\text{YVO}_4:\text{Eu}^{3+}$, further confirming the formation of nanocrystalline layers of $\text{YVO}_4:\text{Eu}^{3+}$ on SiO_2 spheres.

The strong luminescence of Eu^{3+} results from an efficient energy transfer from the VO_4^{3-} group to Eu^{3+} in $\text{YVO}_4:\text{Eu}^{3+}$ layers of the core-shell phosphors as reported previously.^{23–25,34–35} The energy-transfer process from VO_4^{3-} to Eu^{3+} as well as the emission process of Eu^{3+} is schematically shown in Figure 7. To obtain more information about the energy transfer process from VO_4^{3-} to Eu^{3+} , time-resolved emission spectra of Eu^{3+} in the $\text{YVO}_4:\text{Eu}^{3+}@\text{SiO}_2$ core-shell phosphors were recorded at room temperature by exciting into the absorption of VO_4^{3-} using a 278-nm laser with delay time ranging from 1 to 1000 μs , as shown in Figure 8. Clearly, the emission of Eu^{3+} increases from $t = 1$ to 20 μs , then begins to decay from $t = 20$ to 40 μs until $t = 1000\text{ }\mu\text{s}$. The initial increase for the luminescence of Eu^{3+} within 20 μs is in good agreement with the result for nanocrystalline $\text{YVO}_4:\text{Eu}^{3+}$ powder²⁵ and can be attributed to the finite transfer time involved in the $\text{VO}_4^{3-} \rightarrow \text{Eu}^{3+}$ energy-transfer process and the population of the ${}^5\text{D}_0$ level via the higher level (${}^5\text{D}_1$) after energy transfer, as schematically shown in Figure 7. It has been reported that the $\text{VO}_4^{3-} \rightarrow \text{Eu}^{3+}$ energy transfer is dominated by exchange interaction at room temperature, and $\text{VO}_4^{3-} \rightarrow \text{Eu}^{3+}$ energy transfer rate is of the order of 10^7 s^{-1} ($10\text{ }\mu\text{s}^{-1}$),³⁶ which is much faster than the radiative rate of Eu^{3+} (${}^5\text{D}_0$, $10^3\text{--}10^4\text{ s}^{-1}$).²³ As a result, the excited state of Eu^{3+} (${}^5\text{D}_0$) can be populated many times ($10\text{ }\mu\text{s}^{-1} \times 20\text{ }\mu\text{s} = 200$) by the energy transfer from VO_4^{3-} before the depopulation occurs, resulting in the increase of emission intensity during

(32) Blasse, G.; Bril, A. *Philips Res. Repts.* **1966**, *2*, 368.

(33) Blasse, G.; Grabmaier, B. C. *Luminescent Materials*; Springer-Verlag: Berlin, Heidelberg, 1994; Chapter 4.

(34) Venikouas G. E.; Powell, R. C. *J. Lumin.* **1978**, *16*, 29.

(35) Kang, W. Y.; Park, J. S.; Kim, D. K.; Suh, K. S. *Bull. Korean Chem. Soc.* **2001**, *22*, 921.

(36) Blasse, G. *Philips Res. Repts.* **1969**, *24*, 131. Blasse, G.; Bril, A. *Philips Technol. Rev.* **1970**, *31*, 304.

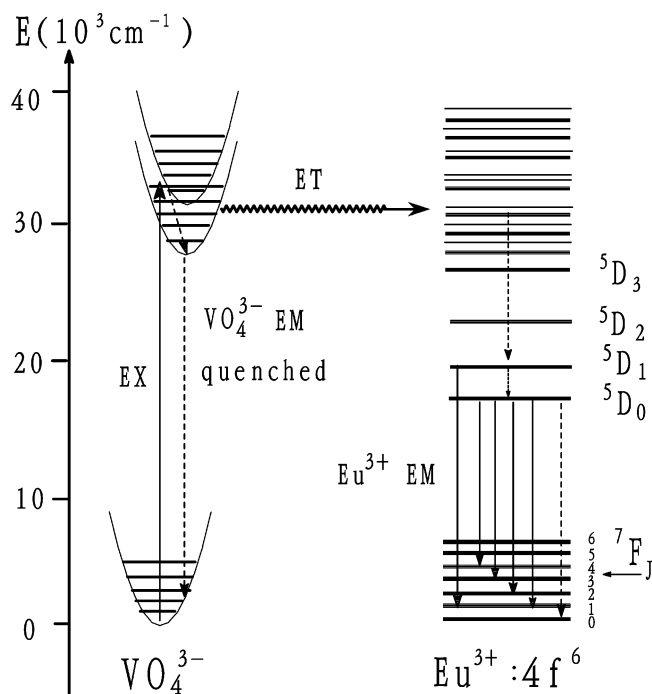


Figure 7. The diagram for $\text{VO}_4^{3-} \rightarrow \text{Eu}^{3+}$ energy transfer and Eu^{3+} emission process.

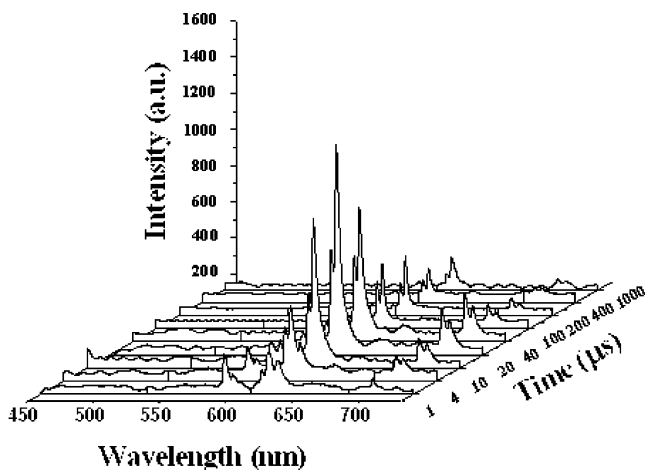


Figure 8. Time-resolved emission spectra of Eu^{3+} in the $\text{YVO}_4:\text{Eu}^{3+}@\text{SiO}_2$ sample ($\lambda_{\text{ex}} = 278$ nm laser).

this period. From Figure, 8 it can also be seen that for $t = 1 \mu\text{s}$ the ${}^5\text{D}_0\text{--}{}^7\text{F}_2$ and ${}^5\text{D}_0\text{--}{}^7\text{F}_1$ of Eu^{3+} nearly have equal intensity [$I({}^5\text{D}_0\text{--}{}^7\text{F}_2)/I({}^5\text{D}_0\text{--}{}^7\text{F}_1)$], namely, $\text{R/O} \approx 1$], and with the increase of delay time (4–20 μs), ${}^5\text{D}_0\text{--}{}^7\text{F}_2$ becomes much stronger than ${}^5\text{D}_0\text{--}{}^7\text{F}_1$ ($\text{R/O} \gg 1$). This just reflects the allowed feature of ${}^5\text{D}_0\text{--}{}^7\text{F}_2$ transition of Eu^{3+} in the YVO_4 host lattices.

To study the decay behaviors of Eu^{3+} luminescence in more details in the $\text{YVO}_4:\text{Eu}^{3+}@\text{SiO}_2$ core–shell phosphors, the kinetic curves for the representative emission of Eu^{3+} ${}^5\text{D}_1\text{--}{}^7\text{F}_1$ (538 nm) and ${}^5\text{D}_0\text{--}{}^7\text{F}_2$ (617 nm, main emission) were measured, as shown in parts a and b of Figure 9, respectively. The decay curve for ${}^5\text{D}_1\text{--}{}^7\text{F}_1$ (538 nm) of Eu^{3+} (Figure 9a) can be well fitted into single-exponential function as $I = A \exp(-t/\tau)$, and the fitting parameters are shown inside the figure. A lifetime τ value of 8.49 μs is obtained for ${}^5\text{D}_1\text{--}{}^7\text{F}_1$ (538 nm) emission of Eu^{3+} , agreeing well with the results for Eu^{3+} in nanocrystalline thin film (7.1 μs for

${}^5\text{D}_1\text{--}{}^7\text{F}_1$)³⁵ and powder (6.6 μs for ${}^5\text{D}_1\text{--}{}^7\text{F}_2$)²⁵ of $\text{YVO}_4:\text{Eu}^{3+}$. However, the decay curve for main emission ${}^5\text{D}_0\text{--}{}^7\text{F}_2$ (617 nm) of Eu^{3+} (Figure 9b) cannot fit into the single-exponential function like the ${}^5\text{D}_1\text{--}{}^7\text{F}_1$ emission but can be well fit into a double-exponential function as $I = A_1 \exp(-t/\tau_1) + A_2 \exp(-t/\tau_2)$, and the fitting results are shown inside Figure 9b. Two lifetimes, a fast one, $\tau_1 = 134 \mu\text{s}$, and a slow one, $\tau_2 = 729 \mu\text{s}$, have been obtained for ${}^5\text{D}_0\text{--}{}^7\text{F}_2$ emission of Eu^{3+} . The double-exponential decay behavior of the activator is frequently observed when the excitation energy is transferred from the donor.^{37,38} A very similar situation was observed in the nanocrystalline $\beta\text{-Ga}_2\text{O}_3:\text{Dy}^{3+}$ system, where an efficient energy transfer occurred from the $\beta\text{-Ga}_2\text{O}_3$ host to Dy^{3+} like $\text{YVO}_4:\text{Eu}^{3+}$, and a double-exponential decay of Dy^{3+} emission was observed upon exciting into $\beta\text{-Ga}_2\text{O}_3$ host at 254 nm.³⁸ Hsu and Powell³¹ proposed a model for the luminescence and energy transfer in $\text{YVO}_4:\text{Eu}^{3+}$ and predicted that the activator (Eu^{3+}) luminescence can exhibit either a double decay or an initial rise in the emission followed by a decay upon excitation into the VO_4^{3-} absorption band of the host. Our results are consistent with this model, i.e., both the double decay (${}^5\text{D}_0\text{--}{}^7\text{F}_2$, Figure 9b) and the initial rise in the emission followed by a decay (time-resolved emission spectra in Figure 8) have been observed in the $\text{YVO}_4:\text{Eu}^{3+}@\text{SiO}_2$ core–shell phosphors. The average lifetime of Eu^{3+} ${}^5\text{D}_0\text{--}{}^7\text{F}_2$ emission, defined as $\langle \tau \rangle = (A_1\tau_1^2 + A_2\tau_2^2)/(A_1\tau_1 + A_2\tau_2)$,³⁷ can be determined to be 648 μs , which is basically in accord with the literature values given for the bulk (525 μs ²³ and 475 μs ³⁴) and nanocrystalline (740 μs ²⁵) $\text{YVO}_4:\text{Eu}^{3+}$ materials.

Tuning of the PL Intensity in the $\text{YVO}_4:\text{Eu}^{3+}@\text{SiO}_2$ Core–Shell Phosphors. The photoluminescence intensity of $\text{YVO}_4:\text{Eu}^{3+}@\text{SiO}_2$ core–shell phosphors can be tuned by several experimental factors, such as annealing temperature, PEG concentration in the precursor solution, and the number of coatings. Figure 10 shows photoluminescence intensity of the core–shell phosphor as a function of annealing temperature. Clearly, the PL intensity increases with raising the annealing temperature from 300 to 700 $^\circ\text{C}$. This is a common phenomenon due to the improvement of crystallinity of $\text{YVO}_4:\text{Eu}^{3+}$ shells with raising the annealing temperature.²²

The $\text{YVO}_4:\text{Eu}^{3+}@\text{SiO}_2$ core–shell phosphors also show different PL intensity when the PEG concentration was changed in the precursor solutions. Figure 11 exhibits the photoluminescence intensity of the sample as function of the PEG concentration in the precursor solutions. The photoluminescence intensity of Eu^{3+} first increases with the increase of PEG concentration from 0.04 to 0.08 g/mL, reaching a maximum at PEG concentration = 0.08 g/mL, then decreases gradually until the PEG concentration increases to 0.20 g/mL. In the precursor solution, the citric acid can form chelates with the metal ions (Y^{3+} , Eu^{3+}). These chelates can be bonded together to form a polymer when

(37) Fujii, T.; Kodaira, K.; Kawauchi, O.; Tanaka, N.; Yamashita, H.; Anpo, M. *J. Phys. Chem. B* **1997**, *101*, 10631. Murakami, S.; Herren, M.; Rau, D.; Morita, M. *Inorg. Chim. Acta* **2000**, *300–302*, 1014.

(38) Shen, W. Y.; Pang, M. L.; Lin, J.; Fang, J. Y. *J. Electrochem. Soc.* **2005**, *152*, H25.

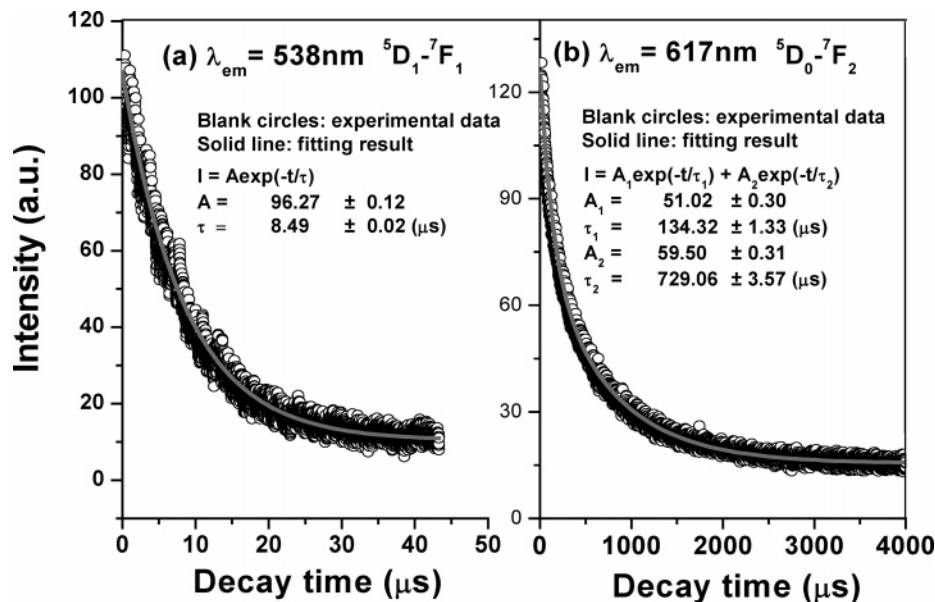


Figure 9. The decay curves for the ${}^5D_1-{}^7F_1$ (538 nm) and ${}^5D_0-{}^7F_2$ (617 nm) emission of Eu^{3+} in the $\text{YVO}_4:\text{Eu}^{3+}@\text{SiO}_2$ sample annealed at 500 °C ($\lambda_{\text{ex}} = 278$ nm laser).

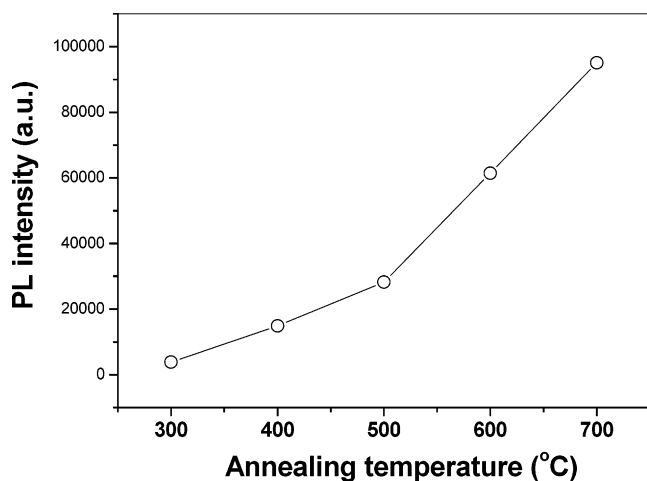


Figure 10. The photoluminescence emission intensity of Eu^{3+} in $\text{YVO}_4:\text{Eu}^{3+}@\text{SiO}_2$ sample as a function of annealing temperatures.

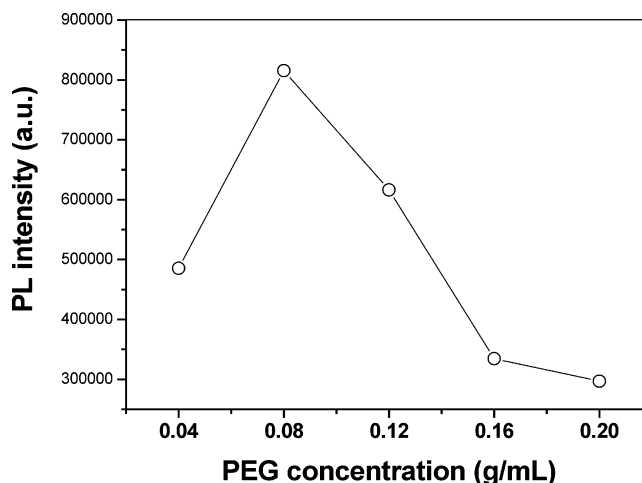


Figure 11. The photoluminescence emission intensity of Eu^{3+} in $\text{YVO}_4:\text{Eu}^{3+}@\text{SiO}_2$ sample as function of the PEG concentration in the precursor solutions.

PEG is added (the two $-\text{OH}$ groups in PEG can connect with the $-\text{COOH}$ groups in citric acid via hydrogen bonding, making them more homogeneously distributed in the solution). The PEG concentration will affect the viscosity of the polymer sol solution. Low viscosity of the sol will result in easy deposition of a thin layer of $\text{YVO}_4:\text{Eu}^{3+}$ on the SiO_2 particles, and proper increase of sol viscosity can increase the thickness of $\text{YVO}_4:\text{Eu}^{3+}$ layer followed by the increase of PL intensity. However, when the sol viscosity exceeds a critical value, it will be difficult for the sol to be coated on the SiO_2 particles homogeneously and more organic impurities (such as $-\text{OH}$, $-\text{OR}$, $-\text{CH}_2$, etc.) will be introduced on the SiO_2 particles. These impurities might not be removed completely in the following annealing process and impair the photoluminescence intensity.^{22,39} It is found from our experiment that the optimum PEG concentration is 0.08 g/mL, which yields the highest photoluminescence intensity for the resulting phosphors.

Another important factor affecting the photoluminescence intensity of the sample is the number of the coatings (N). The photoluminescence intensity increases with the increase of the coating number, as shown in Figure 12. Obviously this can be attributed to the increase of the thickness of $\text{YVO}_4:\text{Eu}^{3+}$ shells on the SiO_2 spheres. The photoluminescence intensity of four-layer $\text{YVO}_4:\text{Eu}^{3+}$ coated SiO_2 core-shell phosphor can reach about 70% that of the pure $\text{YVO}_4:\text{Eu}^{3+}$ powder phosphor as indicated in Figure 12.

IV. Conclusions

An effective and simple sol-gel process has been developed to deposit $\text{YVO}_4:\text{Eu}^{3+}$ layers on SiO_2 spheres. The obtained $\text{YVO}_4:\text{Eu}^{3+}@\text{SiO}_2$ core-shell phosphors have spherical morphology, sub-micrometer size, and narrow size distribution. The spectral and kinetic properties of the core-shell phosphors are similar to those of the reported bulk and nanocrystalline $\text{YVO}_4:\text{Eu}^{3+}$ phosphors. The photoluminescence intensity of the core-shell phosphors can be tuned

(39) Zhou, Y. H.; Lin, J.; Wang, S. B.; Zhang, H. J. *Opt. Mater.* **2002**, *20*, 13.

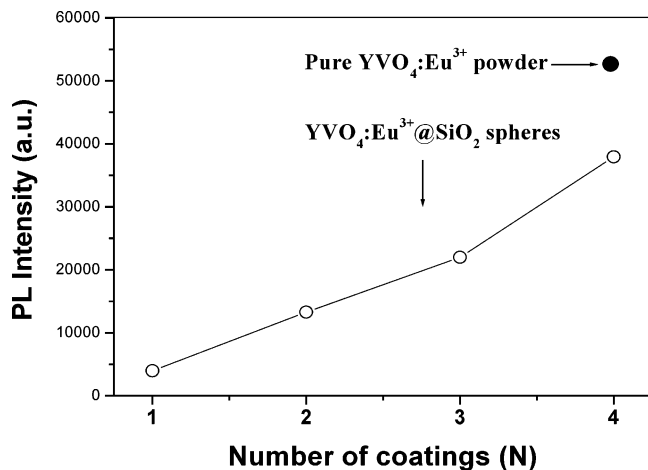


Figure 12. The photoluminescence emission intensity of Eu^{3+} as a function of the number of coatings (N) of $\text{YVO}_4:\text{Eu}^{3+}$ on SiO_2 particles. The photoluminescence intensity of pure $\text{YVO}_4:\text{Eu}^{3+}$ powder is also given.

by the annealing temperature, PEG concentration in the precursor solutions, and the number of coatings. With the

increase of annealing temperature and the number of coatings, the photoluminescence intensity increases. The optimum concentration for PEG in the precursor solution is determined to be 0.08 g/mL. The current method can be extended to prepare various other core-shell phosphors with homogeneous morphology and decrease the cost of phosphors to some degree.

Acknowledgment. This project is financially supported by the foundation of “Bairen Jihua” of Chinese Academy of Sciences, the MOST of China (2003CB314707), the National Natural Science Foundation of China (NSFC, 50225205, 20271048, 20431030), and the Outstanding Youth Fund of Jilin Province (2001). Prof. J. Fang is grateful for the financial support by the foundation of a two-base program for international cooperation of NSFC (00310530) related to Project 50225205, and NSF DMR-0449580. We are grateful for Prof. Yingning Yu and Mr. Liaohai Ge for measuring the time-resolved emission spectra, SEM, and TEM, respectively.

CM0479537